Water in Inhomogeneous Nanoconfinement: Coexistence of Multilayered Liquid and Transition to Ice Nanoribbons

Hu Qiu,*,† Xiao Cheng Zeng,*,‡ and Wanlin Guo*,†

†Key Laboratory for Intelligent Nano Materials and Devices of MOE and State Key Laboratory of Mechanics and Control of Mechanical Structures, Institute of Nano Science, Nanjing University of Aeronautics and Astronautics, Nanjing 210016, China and ‡Department of Chemistry and Nebraska Center for Materials and Nanoscience, University of Nebraska—Lincoln, Lincoln, Nebraska 68588, United States

ABSTRACT Phase behavior and the associated phase transition of water within inhomogeneous nanoconfinement are investigated using molecular dynamics simulations. The nanoconfinement is constructed by a flat bottom plate and a convex top plate. At 300 K, the confined water can be viewed as a coexistence of monolayer, bilayer, and trilayer liquid domains to accommodate the inhomogeneous confinement. With increasing liquid density, the confined water with uneven layers transforms separately into two-dimensional ice crystals with unchanged layer number and rhombic in-plane symmetry for oxygen atoms. The monolayer water undergoes the transition first into a puckered ice nanoribbon, and the bilayer water transforms into a rhombic ice nanoribbon next, followed by the transition of trilayer water into a trilayer ice nanoribbon. The sequential localized liquid-to-solid transition within the inhomogeneous confinement can also be achieved by gradually decreasing the temperature at low liquid densities. These findings of phase behaviors of water under the inhomogeneous nanoconfinement not only extend the phase diagram of confined water but also have implications for realistic nanofluidic systems and microporous materials.

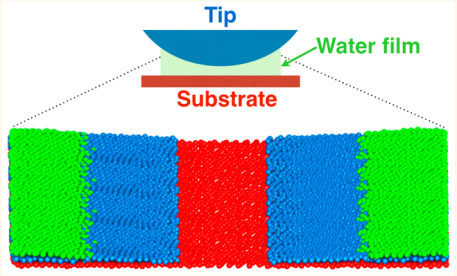

KEYWORDS: inhomogeneous nanoconfinement · phase behavior · molecular dynamics · ice nanoribbon

When confined within nanoscale spaces such as between two parallel solid plates separated by a few molecular layers, water/ice properties such as diffusivity and crystal symmetry can be dramatically different from those of bulk water/ice. On freezing, confined water is thermodynamically more favorable to be solidified due to confinement-reduced translational entropy. As an example, the viscosity of water confined between a gold tip of an interfacial force microscopy and a gold substrate at room temperature is 7 orders of magnitude higher than that of the bulk,[1] implying the possible occurrence of confinement-induced phase transition. Using a friction force microscope with a sharp tungsten tip scanning over a graphite surface, Jinesh and Frenken reported the stick—slip motion of the tip at certain humidities with a spatial period distinct from the graphite lattice, and they attributed this signal to confinement-induced formation of ice at room temperature.[2] Khan *et al.* detected solidification of confined water, as indicated by a sharp transition from viscous to elastic response when compressed to a few molecular layers.[3] The structure of two-dimensional free-standing ice was first predicted by Koga *et al.* through molecular dynamics (MD) simulation,[4] namely, bilayer hexagonal crystalline ice formed between two parallel hydrophobic surfaces. Monolayer square ice, either in puckered or flat form, was also observed in MD simulations.[5,6] Later simulations continued to predict novel structural and dynamic behaviors of two-dimensional confined water.[7−15] More recently, single- and multilayer square ices were directly observed between two graphene sheets in experiments.[16] All the reported two-dimensional ice structures differ from those of known bulk ice polymorphs.

Thus far, nearly all previous MD simulation studies of confined water are based on

* Address correspondence to qiuhu@nuaa.edu.cn, xzeng1@unl.edu, wlguo@nuaa.edu.cn.

Received for review May 27, 2015 and accepted September 8, 2015.

Published online September 08, 2015
10.1021/acsnano.5b04947

homogeneous confining geometries that typically consist of two parallel flat plates. However, the two-dimensional confining spaces in realistic experiments are generally not perfectly homogeneous. For instance, the water layer between the tip of an interfacial force microscopy and a gold substrate was considered to be a meniscus,[1] as the tip end of scanning probe microscopes is generally not a flat plane but a convex one.[17−21] Moreover, water layers confined to biological systems such as within the internal region of antifreeze proteins[22] or within thin junctions between lens fiber cells[23] are also subjected to inhomogeneous confinement.

In this study, we report, to our knowledge, the first comprehensive MD simulation study of water behavior under two-dimensional inhomogeneous confinement in atomic detail. We demonstrate intriguing phase behaviors and particularly associated phase transition of water confined to an inhomogeneous slit that consists of a convex plate and a flat plate, resembling inhomogeneous interspacing between a microscope tip and a flat substrate. In our system, water at low densities exhibits three coexisting liquid domains (or "phases"), *i.e.*, monolayer, bilayer, and trilayer. With increasing liquid density in the slit, the liquid transforms into a coexisting "multiphase", *i.e.*, monolayer, bilayer, and trilayer ice nanoribbons. The transition occurs sequentially in the order of monolayer, bilayer, and trilayer ice nanoribbons from the narrow center region to the wide edge region of the system. Comparative analyses between the present inhomogeneous system and the widely studied homogeneous system reveal the transverse transfer of water from the highly confined center region to the weakly confined edge region in the inhomogeneous system during the density increase. Another independent series of MD simulations indicate that decreasing the temperature at low densities can also induce sequential localized freezing transitions in the inhomogeneous slit.

RESULTS AND DISCUSSION

A schematic illustration of the simulation system is shown in Figure 1a. To introduce the inhomogeneous nanoconfinement, water is held between a flat bottom plate and a convex top plate. It has been shown that, from numerous previous simulation studies, water exhibits different phases with a layered configuration when subjected to various homogeneous nanoconfinements, including monolayer water or ice, bilayer water or ice, trilayer water,[5,7−15,24] *etc*. In the present inhomogeneous nanoconfinement, different phase behaviors arise as indicated by distinct features in lateral diffusion coefficient contour plots shown in Figure 1b. For the low density ρ = 0.92 g/cm^3, the system exhibits an apparent uniform distribution of diffusion coefficient on the order of 10^{-5} cm^2/s (see the first panel in Figure 1b), comparable to that of bulk liquid TIP5P water.[25] However, closer examination of the MD trajectory indicates that the system is actually inhomogeneous, which can be viewed as the coexistence of at least three distinct liquid water domains: monolayer (zone I), bilayer (zone II), and trilayer (zone III). This view is further supported by the vertical density distribution of water in different regions (discussed below). Upon increasing the density to 1.08 g/cm^3, the diffusivity of trilayer water in zone III seems unchanged (see the second panel in Figure 1b). Surprisingly, a sudden drop in diffusivity by 3 orders of magnitude occurs in zone I, reflecting a freezing transition of the monolayer from water to an ice nanoribbon. In addition, a slight decrease of diffusivity occurs in zone II at this density. A further increase of density to 1.13 g/cm^3 can induce the freezing of the bilayer in zone II, while the water diffusivities in zones I and III are still unaffected (see the third panel in Figure 1b). When the density is

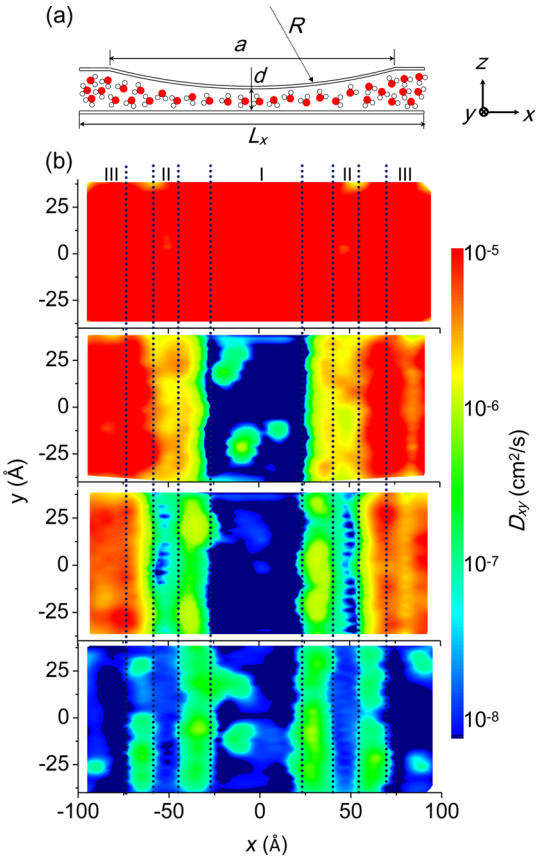

Figure 1. Phase behavior of water under inhomogeneous confinement at 300 K. (a) Schematic of the simulation system consisting of liquid water sandwiched between a flat bottom plate and a convex top plate with a tip radius R = 80 nm. Other geometric parameters were chosen as a = 165 Å, L_x = 195 Å, and L_y = 78 Å. (b) Contour plot of lateral diffusion coefficient D_{xy} of water under different densities ρ = 0.92, 1.08, 1.13, and 1.24 g/cm^3 (from top to bottom), at R = 80 nm and d = 7.32 Å. Zones I to III correspond to different water/ice domains: monolayer, bilayer, and trilayer, respectively. The coordinate origin was placed at the center of the simulation system.

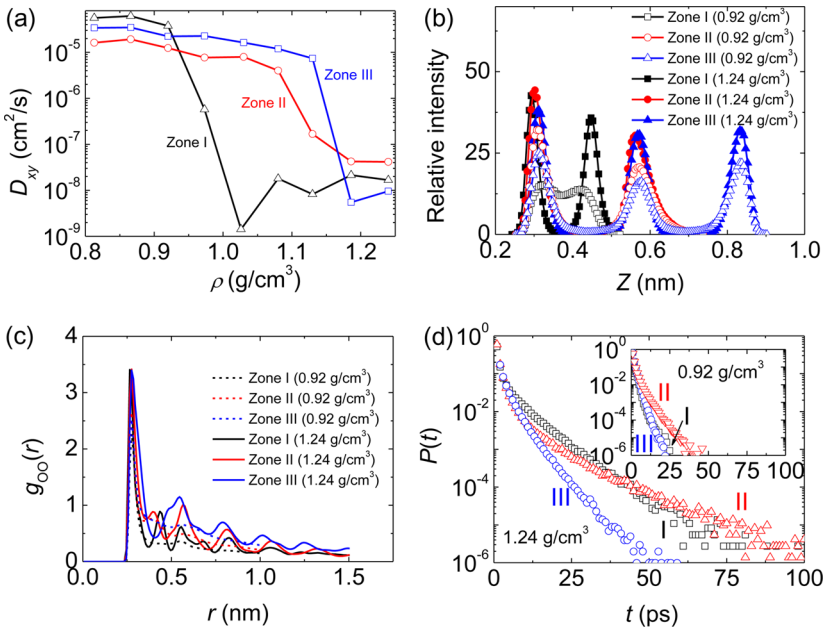

Figure 2. Dynamics of water in each zone of the inhomogeneous confinement under different densities. (a) Averaged lateral diffusion coefficient D_{xy} of water in different zones as a function of density ρ. (b) Vertical density distribution (along the z direction) of water oxygen atoms in different regions at ρ = 0.92 and 1.24 g/cm^3. (c) Oxygen−oxygen radial distribution function $g_{OO}(r)$ in different zones at ρ = 0.92 and 1.24 g/cm^3. (d) Probability distribution $P(t)$ of hydrogen bond lifetime in water at different zones at ρ = 1.24 g/cm^3. Inset shows the same profile but at ρ = 0.92 g/cm^3.

increased to 1.24 g/cm^3, the freezing of the bilayer in zone II can be promoted significantly, as shown by lower diffusivity in this zone (see the fourth panel in Figure 1b). At this density, we also observed the freezing transition of the trilayer water in zone III located at the boundary of the simulation system. Eventually, the system transforms from an inhomogeneous liquid containing monolayer, bilayer, and trilayer water at a lower density to an inhomogeneous solid containing monolayer, bilayer, and trilayer ice nanoribbons at a higher density.

If either tip radius (Figure S1c) or plate separation (Figure S1d) changes slightly, the coexistence of monolayer, bilayer, and trilayer water/ice domains can still be seen, as well as the transition from liquid to solid with increasing water densities, although the specific region and the transition sequence for different water layers may vary (see Section 1 of the Supporting Information for more details).

To describe the "phase" transition in different domains of the inhomogeneous water system, we show in Figure 2a the averaged diffusion coefficient in the three domains as a function of water density. With an increase of the density, zone I transfers into a solid phase first at ρ = 1.026 g/cm^3, while zone II is the second at ρ = 1.13 g/cm^3, followed by zone III at ρ = 1.184 g/cm^3. The demand of a higher critical density of zone II than zone I to complete the transition agrees with the relatively higher pressure required to solidify a bilayer liquid[6] than that to solidify a monolayer liquid.[14]

When water is placed adjacent to the solid walls, layering of water is induced due to water−wall interactions. Such a layering phenomenon can be validated through the conspicuous peaks in the vertical density profile of oxygen at liquid densities of 0.92 g/cm^3 (empty symbols in Figure 2b) and 1.24/cm^3; filled symbols in Figure 2b). At the lower density 0.92 g/cm^3 and in zone I, two fused peaks can be seen in Figure 2b, suggesting a monolayer configuration of liquid water. At the higher density of 1.24 g/cm^3, the peaks in zone I become more apparent and a deep valley between the two peaks arises. Examination of the MD trajectory suggests that the system exhibits a monolayer ice nanoribbon with a puckered structure, consistent with previous studies based on homogeneous confinement.[5,26] In zones II and III, the local water clearly exhibits a bilayer and trilayer configuration, respectively. But contrary to the abrupt change in zone I, only a slight decrease in peak heights was observed for the vertical density profiles in zones II and III (see Figure 2b), while peak positions remain nearly unchanged with increasing density. In Figure 2c, we plotted oxygen−oxygen radial distribution functions (RDFs) at liquid densities of 0.92 and 1.24 g/cm^3, respectively. At 0.92 g/cm^3, the short-range ordering in the RDFs suggests that the system is in a liquid state for all three zones (dashed lines in Figure 2c). At the high density of 1.24 g/cm^3, well-defined maxima and minima can be seen in all three RDFs (solid lines in Figure 2c), suggesting that the system becomes a solid, including monolayer, bilayer, and trilayer ice nanoribbons. Shown in Figure 2d are the probability distributions of the hydrogen bond lifetime for water in three zones at the two densities. It is found that the probability

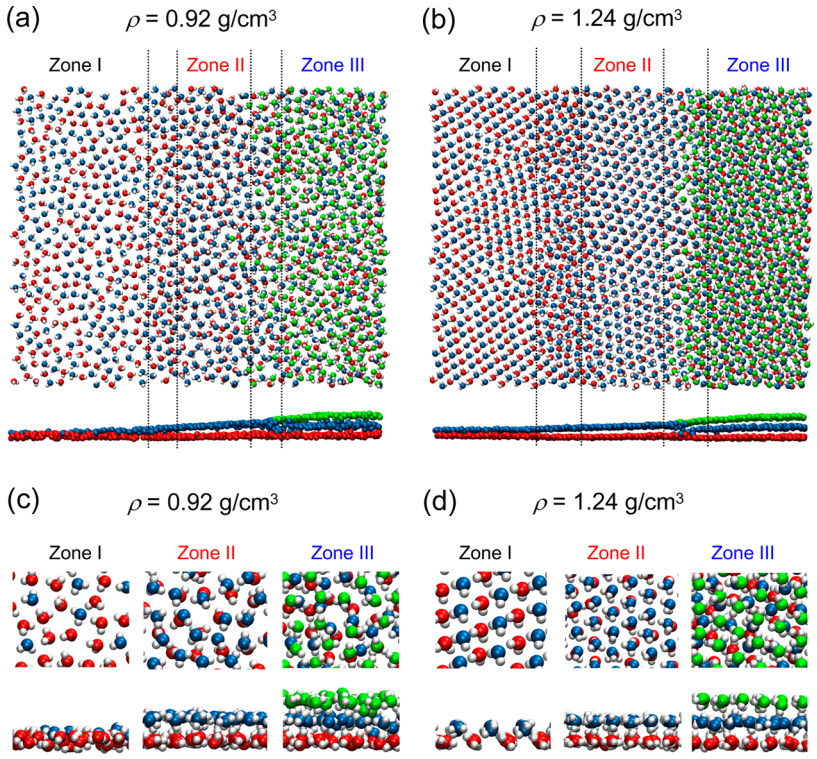

Figure 3. Snapshots from MD simulations showing coexisting domains of water/ice nanoribbons. (a, b) In-plane and out-of-plane views of the right half ($x > 0$) of the inhomogeneous water (symmetric with respect to the plane at $x = 0$) at liquid densities $\rho = 0.92$ g/cm^3 (a) and 1.24 g/cm^3 (b). White spheres represent hydrogen, while green, blue, and red spheres represent the top, middle, and bottom water oxygen planes, respectively. Definition of water planes is based on the location of minima in vertical density profiles shown in Figure 2b. For clarity, hydrogen atoms are not shown in the out-of-plane views. (c, d) Enlarged images showing three coexisting water domains or ice nanoribbons at densities of $\rho = 0.92$ g/cm^3 (c) and 1.24 g/cm^3 (d).

distribution decays much slower at higher density (Figure 2d) than at lower density (Figure 2d inset). This result further confirms the liquid-to-solid transition of water in the inhomogeneous confinement.

Figure 3a and b show snapshots of the system at $\rho =$ 0.92 and 1.24 g/cm^3, respectively, where the layering effect of oxygen planes can be clearly seen from the side view of the system. The structures of water in three oxygen planes along the z direction [bottom (red), middle (blue), and top (green)] are also shown in Figure S2b–d, f–h for $\rho = 0.92$ and 1.24 g/cm^3, respectively. Five different types of water/ice nanoribbons can be clearly seen from both the MD snapshots, including monolayer (zone I), bilayer (zone II), and trilayer (zone III), and the transition regions between adjacent zones. This result is consistent with the observation from the lateral diffusion coefficient distribution (Figure 1b). In zone I, water molecules exhibit a disordered monolayer liquid configuration (left panel in Figure 3c). With increasing density, the monolayer transforms to a puckered monolayer ice nanoribbon (left panel in Figure 3d), as indicated by the two separated peaks in the vertical density profile (Figure 2b). Within the monolayer ice nanoribbon, every water molecule can form two hydrogen bonds with its neighboring water molecules in the same water plane and another two hydrogen bonds with its neighboring water molecules in the opposing plane, consistent with previous studies.[5,26] Note that, in zone I, water exhibits a lower in-plane density than that in zones II and III, regardless of the overall density of the system (see Figure S2i and j), further validating the monolayer structure of water/ice in this region. In zone II, comparison between low-density (middle panel in Figure 3c) and high-density (middle panel in Figure 3d) snapshots indicates that the high-density structure is an ice nanoribbon with rhombic in-plane symmetry of oxygen atoms (see also Figure S2f and g), while the low-density structure is a liquid without any in-plane symmetry of oxygen atoms (see also Figure S2b and c). Moreover, in the high-density bilayer ice nanoribbon of zone II, oxygen atoms in one plane are in registry with oxygen atoms in another plane, whereas such kind of position registry for oxygen atoms is not common in the low-density water system. In zone III, again, the high-density structure is a trilayer ice nanoribbon (right panel in Figure 3d), whereas the low-density structure is a trilayer liquid (right panel in Figure 3c). In the ice structure, however, the position registry for oxygen atoms disappears (right panel in Figure 3d).

To clarify the main difference in water behaviors between the present inhomogeneous system and those in the widely studied homogeneous system, we carried out additional simulations on homogeneous systems

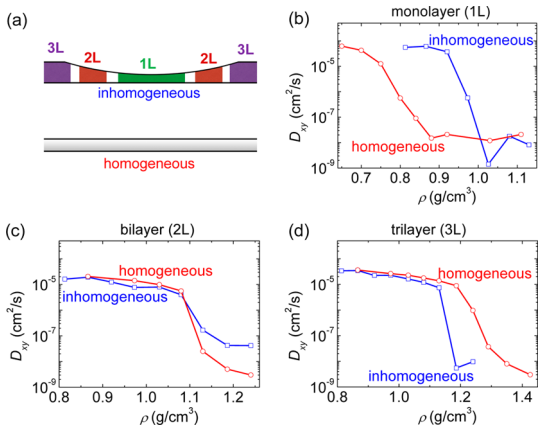

Figure 4. Comparison in phase transition between inhomogeneously confined water and homogeneously confined water. (a) Schematic of an inhomogeneous system (top) containing coexisting monolayer, bilayer, and trilayer water/ice domains and a homogeneous system (bottom) containing a uniform water phase. The homogeneous system containing a monolayer, bilayer, and trilayer phase has a plate separation of 7.67, 9.00, and 11.50 Å, respectively. (b–d) Comparison in lateral diffusion coefficient D_{xy} of monolayer (b), bilayer (c), and trilayer (d) water/ice between the inhomogeneous confinement (blue lines) and the homogeneous confinement (red lines).

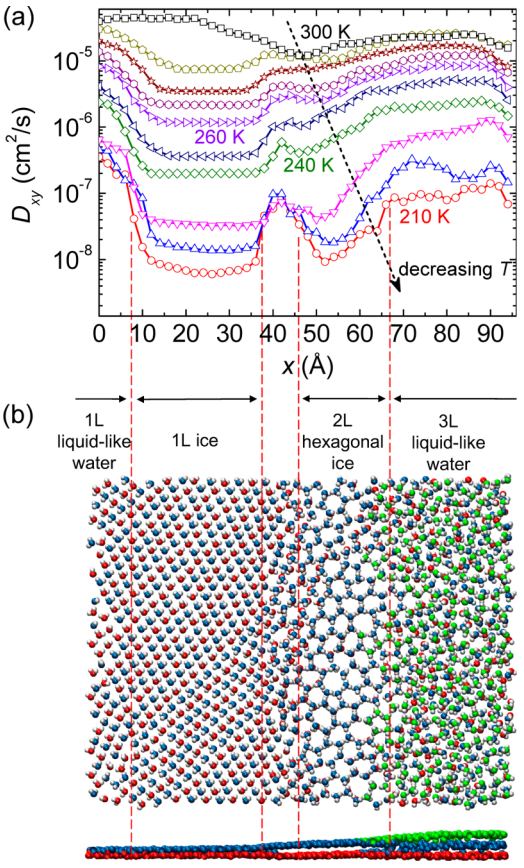

Figure 5. Phase transition of water in inhomogeneous confinement at a density of ρ = 0.92 g/cm^3 when gradually decreasing the temperature T from 300 to 210 K. (a) Average lateral diffusion coefficient D_{xy} of water as a function of position x for the right half of the water system under different T. (b) In-plane (top) and out-of-plane (bottom) views of the right half of inhomogeneous water at T = 210 K.

(consisting of two parallel and flat plates; see bottom panel in Figure 4a) and compared the newly obtained results with those of the inhomogeneous system (consisting of a flat plate and a convex plate; top panel in Figure 4a). We compared the diffusion coefficient of each water/ice phase between the convex plate system and the flat plate system. For monolayer water/ice, the solidification in the inhomogeneous convex plate system occurs at densities of 0.92–1.026 g/cm^3, much higher than those (0.75–0.88 g/cm^3) in the homogeneous flat plate system (Figure 4b). The higher transition density in the convex plate system can be attributed to the spatial inhomogeneity. Specifically, water in the highly confined monolayer domain tends to be squeezed into nearby weakly confined regions (*e.g.*, the transition zone between monolayer and bilayer) to offset partly the increase in overall densities. In the case of the bilayer domain, however, the solidification in the two systems arises at nearly the same densities of 1.08–1.13 g/cm^3 (Figure 4c). In stark contrast to the monolayer, the solidification of the trilayer in the inhomogeneous convex plate system occurs at densities of 1.13–1.186 g/cm^3, slightly lower than those (1.186–1.29 g/cm^3) in the homogeneous system (Figure 4d). The lower critical density in the convex plate system could be attributed again to the spontaneous transverse water transfer during density increase. As a result, water squeezed from neighboring highly confined domains (with narrower plate separations) increases the local density of the trilayer domain, leading to a decreased critical solidification density. Although having distinct liquid–solid transition points, each water domain in the inhomogeneous system exhibits structural and dynamic properties similar to those in a homogeneous system.

We have shown that the freezing transition of water in the inhomogeneous confinement can be induced by increasing the water density. Another way to produce a similar transition is to lower the temperature T of the system. Again, we started from the system of coexisting monolayer, bilayer, and trilayer liquid water at density ρ = 0.92 g/cm^3 and T = 300 K. With decreasing T, the lateral diffusion coefficient in all regions of the inhomogeneous system decreases from 10^{-5} cm^2/s at T = 300 K to 10^{-7} or 10^{-8} cm^2/s at T = 210 K (Figure 5a), indicating the occurrence of a freezing transition. Figure 5b shows typical snapshots of water molecules at T = 210 K. In general, several new features can be seen in the low-temperature solid system, compared to the high-density solid system shown in Figure 3b and d. Specifically, water within the narrowest part of the system (central region at x < 7.5 Å) is in a liquid-like state despite the strongest confinement, as indicated by the higher diffusivity (red line in Figure 5a). Previous simulation studies on the flat plate system, although at a different pressure or temperature, also reported the

unexpected presence of a monolayer liquid when excessively decreasing the plate separation to enhance the degree of confinement.[5,27] Next to the liquid-like domain is the monolayer ice nanoribbon (7.5 < x < 37.5 Å) with the same puckered structure (Figure 5b) as in the high-density system (right panel in Figure 3d). However, the most striking structural difference, compared to the high-density system, arises in the region with the bilayer ice nanoribbon (46 < x < 67 Å). The bilayer ice in the high-density system is indeed a room-temperature rhombic bilayer. Note that previous simulation studies predicted the formation of the room-temperature bilayer rhombic ice at a high lateral pressure > ~1 GPa.[14] Recent experiments also confirmed the formation of few-layer rhombic ice at room temperature between graphene sheets at pressures > ~1 GPa induced due to the attractive van der Waals forces between the two sheets.[16] The agreement between previous results and ours arises assuming that pressure increase and density increase have a similar effect on confined water. Instead of having the rhombic symmetry in the high-density case, here the low-temperature bilayer ice nanoribbon exhibits hexagonal rings of water (except a few pentagonal and heptagonal defects). This result agrees well with previous observation of the bilayer hexagonal crystalline (or amorphous) ice at only low temperatures (T < ~270 K).[8,14] In the trilayer region (x > 67 Å), the relatively higher diffusivity indicates that the local water is in a disordered liquid-like state, rather than the ordered trilayer ice nanoribbon seen in the high-density system.

The behavior of water confined between an atomic force microscope (AFM) tip and a substrate surface was believed to have considerable effects on the friction performance when the tip is scanned over the surface in ambient conditions.[28,29] In the work by Jinesh and Frenken, the formation of room-temperature confined ice between a tungsten tip and a graphite surface was found to induce a periodic stick–slip motion of the tip, leading to an evident increase in friction force.[2] The confining geometry of the AFM tip–substrate slit in these experiments should resemble the inhomogeneous confinement studied in this work. We have shown that the distribution and associated transition of water/ice domains within the inhomogeneous confinement are sensitive to the tip curvature, tip–substrate distance, and overall density (pressure) of confined water. It is expected that changes in these experimental conditions would lead to distinct friction behaviors in AFM experiments, providing at least indirect evidence for the present findings. A recent encouraging advancement that may also benefit the experimental realization of the present study is the report of direct high-resolution imaging of few-layer ice confined between two graphene sheets in experiments.[16]

CONCLUSION

In summary, we present a comprehensive study of coexisting water/ice domains in inhomogeneous confinement by MD simulations. The coexistence of monolayer, bilayer, and trilayer domains of liquid water is demonstrated at low water densities. With increasing density, the coexisting water multilayers transform successively into ice nanoribbons from the monolayer region to the bilayer one and finally to the trilayer region. All regions of the coexisting ice domains (except the transition zone between two phases) have rhombic in-plane symmetry for the oxygen atoms. Compared to the homogeneous confinement, the monolayer, bilayer, and trilayer regions exhibit a higher, comparable, and slightly lower freezing density, respectively. This behavior is due to the spontaneous transverse transfer of localized water under inhomogeneous confinement during density increase. Specifically, water in the inhomogeneous system is squeezed from highly confined regions (*e.g.*, monolayer) into weakly confined regions (*e.g.*, trilayer), decreasing local density in the former region but increasing local density in the latter. The freezing transition can also be induced by gradually decreasing the system temperature. The monolayer again freezes into the same rhombic ice nanoribbon, whereas the bilayer water transforms into a bilayer hexagonal ice nanoribbon, and the trilayer water transforms into a liquid-like structure. Our finding of the coexistence and transition of water domains in inhomogeneous confinement not only can enrich the phase diagram of confined water but also have implications for realistic nanofluidic systems and microporous materials.

METHODS

Figure 1a illustrates a schematic diagram of the simulation system of water confined between a flat bottom plate and a convex top plate mimicking an atomic force microscopy tip. The tip radius here (R = 80 or 100 nm) is comparable to the tip radius of curvature of atomic force microscopes. The final dimensions of the system are L_x = 195 Å, L_y = 78 Å, and d = 7.32 Å, where d represents the shortest wall separation. Periodic boundary conditions were applied in the x and y dimensions to model the confinement between two infinite plates, and in the z direction we construct a vacuum layer to prevent interactions of water in adjacent periodic images. To predict properties of water at different densities, a series of independent MD simulations containing 2788–3991 TIP5P water molecules[30] were considered, corresponding to liquid densities of ρ = 0.866–1.24 g/cm^3, respectively. The strategy of varying density to mimic the change in lateral pressure has been widely used to study the behavior of confined water in MD simulations.[10,31] It is expected that, in future AFM experiments to verify our findings, the pressure (water density) could be readily increased (or decreased) by

filling the AFM chamber with compressed gas at a certain high pressure (or evacuating some amount of air from the chamber). Alternatively, a high water density may also be achieved by using a so-called high-pressure AFM that was employed to image supercritical CO_2 at pressures of ~100 atm.[32]

The bottom plate is composed of a triangular arrangement of monolayer atoms, with the neighboring bond length being fixed at 0.23 nm. The *x* and *y* components of each atom position in the convex top plate are also in a triangular arrangement, while *z* components lie on a circle with a radius of *R*. The water−plate (or wall) interactions were modeled by a 6−12 Lennard-Jones (LJ) potential with the parameters $\sigma_{(O\text{-wall})}$ = 0.316 nm, $\sigma_{(H\text{-wall})}$ = 0.284 nm and $\varepsilon_{(O\text{-wall})}$ = 0.831 kJ/mol, $\varepsilon_{(H\text{-wall})}$ = 0.415 kJ/mol, which approximately reproduce the van der Waals (vdW) interaction between a water molecule and a quartz (SiO_2) surface.[5,24]

All MD simulations were carried out using the Gromacs 4.0.5 software package.[33] The NVT ensemble was adopted, with the Berendsen algorithm[34] being used to control the temperature. Without specific statement, the system temperature *T* was fixed at *T* = 300 K. The nonbonded interactions were treated with a cutoff of 0.9 nm. The particle mesh Ewald (PME) method was employed to compute long-range electrostatic interactions.[35] All other simulation parameters were identical to those used in our previous study.[26] Each simulation was equilibrated for 10 ns and then run for another 10−50 ns for data analysis, depending on the simulated density and temperature. In our model, two water molecules were considered to form a H-bond if their O···O distance is shorter than 3.5 Å and simultaneously the angle O−H···O is larger than 150°.

Conflict of Interest: The authors declare no competing financial interest.

Acknowledgment. This work was supported by the 973 Program (2013CB932604, 2012CB933403) and National NSF (11402113, 51472117, 51535005) of China, and Jiangsu NSF (BK20140807). H.Q. acknowledges the support by National and Jiangsu Postdoctoral Research Funds (2014M550288, 1302015B), NUAA Research Fund (1011-YAH13042), Open Fund of Key Laboratory for Intelligent Nano Materials and Devices of the Ministry of Education (INMD-2014M01), and the Fundamental Research Funds for the Central Universities (NJ20140001). X.C.Z. is supported by the US NSF (CHE-1306326, CBET-1512164).

Supporting Information Available: The Supporting Information is available free of charge on the ACS Publications website at DOI: 10.1021/acsnano.5b04947.

Supplementary figures and their legends, effect of confining geometry on water behaviors (PDF)

REFERENCES AND NOTES

1. Major, R. C.; Houston, J. E.; McGrath, M. J.; Siepmann, J. I.; Zhu, X. Y. Viscous Water Meniscus under Nanoconfinement. *Phys. Rev. Lett.* **2006**, *96*, 177803.
2. Jinesh, K. B.; Frenken, J. W. M. Experimental Evidence for Ice Formation at Room Temperature. *Phys. Rev. Lett.* **2008**, *101*, 036101.
3. Khan, S. H.; Matei, G.; Patil, S.; Hoffmann, P. M. Dynamic Solidification in Nanoconfined Water Films. *Phys. Rev. Lett.* **2010**, *105*, 106101.
4. Koga, K.; Zeng, X. C.; Tanaka, H. Freezing of Confined Water: A Bilayer Ice Phase in Hydrophobic Nanopores. *Phys. Rev. Lett.* **1997**, *79*, 5262–5265.
5. Zangi, R.; Mark, A. E. Monolayer Ice. *Phys. Rev. Lett.* **2003**, *91*, 025502.
6. Zhao, W.-H.; Wang, L.; Bai, J.; Yuan, L.-F.; Yang, J.; Zeng, X. C. Highly Confined Water: Two-Dimensional Ice, Amorphous Ice, and Clathrate Hydrates. *Acc. Chem. Res.* **2014**, *47*, 2505–2513.
7. Koga, K.; Tanaka, H.; Zeng, X. C. First-Order Transition in Confined Water Between High-Density Liquid and Low-Density Amorphous Phases. *Nature* **2000**, *408*, 564–567.
8. Koga, K.; Tanaka, H. Phase Diagram of Water between Hydrophobic Surfaces. *J. Chem. Phys.* **2005**, *122*, 104711–10.
9. Kumar, P.; Buldyrev, S. V.; Starr, F. W.; Giovambattista, N.; Stanley, H. E. Thermodynamics, Structure, and Dynamics of Water Confined between Hydrophobic Plates. *Phys. Rev. E* **2005**, *72*, 051503.
10. Giovambattista, N.; Rossky, P. J.; Debenedetti, P. G. Phase Transitions Induced by Nanoconfinement in Liquid Water. *Phys. Rev. Lett.* **2009**, *102*, 050603.
11. Han, S.; Kumar, P.; Stanley, H. E. Hydrogen-Bond Dynamics of Water in a Quasi-Two-Dimensional Hydrophobic Nanopore Slit. *Phys. Rev. E* **2009**, *79*, 041202.
12. Johnston, J. C. Liquid to Quasicrystal Transition in Bilayer Water. *J. Chem. Phys.* **2010**, *133*, 154516.
13. Bai, J.; Angell, C. A.; Zeng, X. C. Guest-Free Monolayer Clathrate and its Coexistence with Two-Dimensional High-Density Ice. *Proc. Natl. Acad. Sci. U. S. A.* **2010**, *107*, 5718–5722.
14. Bai, J.; Zeng, X. C. Polymorphism and Polyamorphism in Bilayer Water Confined to Slit Nanopore under High Pressure. *Proc. Natl. Acad. Sci. U. S. A.* **2012**, *109*, 21240–21245.
15. Zhao, W.-H.; Bai, J.; Yuan, L.-F.; Yang, J.; Zeng, X. C. Ferroelectric Hexagonal and Rhombic Monolayer Ice Phases. *Chem. Sci.* **2014**, *5*, 1757–1764.
16. Algara-Siller, G.; Lehtinen, O.; Wang, F. C.; Nair, R. R.; Kaiser, U.; Wu, H. A.; Geim, A. K.; Grigorieva, I. V. Square Ice in Graphene Nanocapillaries. *Nature* **2015**, *519*, 443–445.
17. Lee, C.; Li, Q.; Kalb, W.; Liu, X.-Z.; Berger, H.; Carpick, R. W.; Hone, J. Frictional Characteristics of Atomically Thin Sheets. *Science* **2010**, *328*, 76–80.
18. Gotsmann, B.; Lantz, M. A. Quantized Thermal Transport across Contacts of Rough Surfaces. *Nat. Mater.* **2012**, *12*, 59–65.
19. Bhaskaran, H.; Gotsmann, B.; Sebastian, A.; Drechsler, U.; Lantz, M. A.; Despont, M.; Jaroenapibal, P.; Carpick, R. W.; Chen, Y.; Sridharan, K. Ultralow Nanoscale Wear through Atom-by-Atom Attrition in Silicon-Containing Diamond-Like Carbon. *Nat. Nanotechnol.* **2010**, *5*, 181–185.
20. De Angelis, F.; Das, G.; Candeloro, P.; Patrini, M.; Galli, M.; Bek, A.; Lazzarino, M.; Maksymov, I.; Liberale, C.; Andreani, L. C.; Di Fabrizio, E. Nanoscale Chemical Mapping using Three-Dimensional Adiabatic Compression of Surface Plasmon Polaritons. *Nat. Nanotechnol.* **2010**, *5*, 67–72.
21. Drew, M. E.; Konicek, A. R.; Jaroenapibal, P.; Carpick, R. W.; Yamakoshi, Y. Nanocrystalline Diamond AFM Tips for Chemical Force Spectroscopy: Fabrication and Photochemical Functionalization. *J. Mater. Chem.* **2012**, *22*, 12682–12688.
22. Sun, T.; Lin, F.-H.; Campbell, R. L.; Allingham, J. S.; Davies, P. L. An Antifreeze Protein Folds with an Interior Network of More Than 400 Semi-Clathrate Waters. *Science* **2014**, *343*, 795–798.
23. Gonen, T.; Cheng, Y.; Sliz, P.; Hiroaki, Y.; Fujiyoshi, Y.; Harrison, S. C.; Walz, T. Lipid-Protein Interactions in Double-Layered Two-Dimensional AQP0 Crystals. *Nature* **2005**, *438*, 633–638.
24. Zangi, R.; Mark, A. E. Bilayer Ice and Alternate Liquid Phases of Confined Water. *J. Chem. Phys.* **2003**, *119*, 1694.
25. Mahoney, M. W.; Jorgensen, W. L. Diffusion Constant of the TIP5P Model of Liquid Water. *J. Chem. Phys.* **2001**, *114*, 363–366.
26. Qiu, H.; Guo, W. Electromelting of Confined Monolayer Ice. *Phys. Rev. Lett.* **2013**, *110*, 195701.
27. Kaneko, T.; Bai, J.; Yasuoka, K.; Mitsutake, A.; Zeng, X. C. New Computational Approach to Determine Liquid−Solid Phase Equilibria of Water Confined to Slit Nanopores. *J. Chem. Theory Comput.* **2013**, *9*, 3299–3310.
28. Binggeli, M.; Mate, C. M. Influence of Capillary Condensation of Water on Nanotribology Studied by Force Microscopy. *Appl. Phys. Lett.* **1994**, *65*, 415–417.
29. Jinesh, K. B.; Frenken, J. W. M. Capillary Condensation in Atomic Scale Friction: How Water Acts like a Glue. *Phys. Rev. Lett.* **2006**, *96*, 166103.
30. Mahoney, M. W.; Jorgensen, W. L. A Five-Site Model for Liquid Water and the Reproduction of the Density Anomaly by Rigid, Nonpolarizable Potential Functions. *J. Chem. Phys.* **2000**, *112*, 8910.

31. Han, S.; Choi, M. Y.; Kumar, P.; Stanley, H. E. Phase Transitions in Confined Water Nanofilms. *Nat. Phys.* **2010**, *6*, 685–689.
32. Lea, A. S.; Higgins, S. R.; Knauss, K. G.; Rosso, K. M. A High-Pressure Atomic Force Microscope for Imaging in Supercritical Carbon Dioxide. *Rev. Sci. Instrum.* **2011**, *82*, 043709.
33. Hess, B.; Kutzner, C.; van der Spoel, D.; Lindahl, E. GROMACS 4: Algorithms for Highly Efficient, Load-Balanced, and Scalable Molecular Simulation. *J. Chem. Theory Comput.* **2008**, *4*, 435–447.
34. Berendsen, H. J. C.; Postma, J. P. M.; van Gunsteren, W. F.; DiNola, A.; Haak, J. R. Molecular Dynamics with Coupling to an External Bath. *J. Chem. Phys.* **1984**, *81*, 3684.
35. Essmann, U.; Perera, L.; Berkowitz, M. L.; Darden, T.; Lee, H.; Pedersen, L. G. A Smooth Particle Mesh Ewald Method. *J. Chem. Phys.* **1995**, *103*, 8577–8593.